

Surface Mechanical Properties of Thin Polymer Films Investigated by AFM  
in Pulsed Force ModeCamila A. Rezende,<sup>‡</sup> Lay-Theng Lee,<sup>§</sup> and Fernando Galembeck<sup>\*;‡</sup><sup>‡</sup>*Institute of Chemistry, University of Campinas – UNICAMP, P.O. Box 6154, CEP 13083-970, Campinas – SP, Brazil, and* <sup>§</sup>*Laboratoire Léon Brillouin, UMR 12, CEA-Saclay, 91191 Gif-sur-Yvette Cedex, France*

Received March 29, 2009. Revised Manuscript Received June 30, 2009

Atomic force microscopy in the pulsed force mode (PFM) is applied in this work to the study of thin dewetting patterns formed by drying an aqueous solution of poly(*N*-isopropylacrylamide) (PNIPAM) and sodium dodecyl sulfate (SDS) on mica. This technique allows the automated acquisition of typically  $4 \times 10^6$  force–distance curves on the sample surface together with maps showing nanodomains differentiated by their stiffness and adhesion to the tip. Topography images of dry films revealed a morphology formed by droplets distributed on the substrate. Adhesion and stiffness images with good lateral resolution show droplets containing polymer and surfactant contrasting with the substrate and also nanosized heterogeneities inside these droplets. They also revealed very small dewetted structures which could not be observed in the topography map by noncontact AFM. Adhesion interactions between the AFM tip and the polymer or the dewetted mica substrate were measured in terms of adhesion force and detachment energy, and can be used as new information to understand dewetting patterns containing silica particles, PNIPAM, and SDS. Other surface mechanical parameters such as stiffness, maximum indentation, hardness, compliance, hysteresis, and Young's modulus were obtained by sampling many points and used to characterize the PNIPAM/SDS films formed in the dewetting process.

## Introduction

Atomic force microscopy (AFM) is one of the most powerful current techniques for surface characterization. Since its introduction in 1986,<sup>1</sup> many improvements have been made to increase image resolution and to minimize damage to the sample as well as imaging artifacts. Different scanning modes and additional modules were developed to extend the technique capabilities. They are based on the different interaction forces between the tip and the sample surface, thus allowing the identification and mapping of domains which are differentiated by electrical, magnetic, thermal, mechanical, and other properties, as well as by their chemical composition. Measurements of force–distance curves, using microscope tip indentation on the sample, emerged as an interesting tool for surface analysis,<sup>2</sup> as the viscoelastic properties in the first surface layers of a material can be very different from the bulk properties.

An AFM force–distance curve is a graph of the tip–sample interaction forces vs the separation distance between them.<sup>3</sup> The experiment consists of measuring the cantilever deflection ( $\delta_c$ ) as the tip moves in the *z* direction, and it is pushed on the sample, until a predefined maximum force is achieved, and then the tip is pulled back. The tip–sample force (*F*) depends on the cantilever deflection according to Hooke's law:  $F = k_c \times \delta_c$ , where  $k_c$  is the spring constant of the cantilever. Single force–distance curves can be measured in different regions of the sample and, as in a typical mechanical test, the greater the number of testing cycles, the better the statistics of the values will be.

Force–distance curves have been used for measurements of the elasticity modulus of materials, for studies on surface wetting properties such as the hydrophobicity degree, for the determination of Hamaker constants between two solids separated by a

fluid media (e.g., silicon, silica, mica through air or water), and for the study of solvation and hydrophobic forces.<sup>3</sup>

The digital pulsed force mode (PFM) is a big step forward in force–distance curves testing, because it is an automated system that is able to measure a very large number of force–distance curves in any given sample (about 3 curves per pixel, depending on the indentation frequency). This results in millions of curves per square micrometer within a reasonable time (about 1 h scanning) and in good statistical significance for the results. It also allows sample imaging, e.g., adhesion and stiffness maps, based on tip–sample adhesion force and sample stiffness values extracted from indentation cycles on each pixel.<sup>4,5</sup> Besides, since the probe scans in intermittent contact and the maximum force between the sample and the tip is controlled within a broad range, PFM is particularly appropriate to analyze soft as well as fragile samples with minimal damage.

PFM has been used to characterize different kinds of systems,<sup>4–15</sup> e.g., adhesive properties of silicon surfaces chemically modified with

(4) Marti, O.; Stifter, T.; Waschpky, H.; Quintus, M.; Hild, S. *Colloids Surf., A* **1999**, *154*, 65–73.

(5) Rosa-Zeiser, A.; Weilandt, E.; Hild, S.; Marti, O. *Meas. Sci. Technol.* **1997**, *8*, 1333–1338.

(6) Csete, M.; Kresz, N.; Vass, Cs.; Kurdi, G.; Heiner, Zs.; Deli, M.; Bor, Zs.; Marti, O. *Mater. Sci. Eng., C* **2005**, *25*, 813–819.

(7) Krottil, H. U.; Stifter, T.; Waschpky, H.; Weiskaupt, K.; Hild, S.; Marti, O. *Surf. Interface Anal.* **1999**, *27*, 336–340.

(8) Segatelli, M. G.; Costa, C. A. R.; Galembeck, F.; Gonçalves, M. C. *Microsc. Microanal.* **2005**, *11*(s3), 134–137.

(9) Roux, S. P.; Jacobs, E. P.; van Reenen, A. J.; Morkel, C.; Meincken, M. *J. Membr. Sci.* **2006**, *276*, 8–15.

(10) Meincken, M.; Klash, A.; Seboa, S.; Sanderson, R. D. *Appl. Surf. Sci.* **2006**, *253*, 805–809.

(11) Kwak, K. J.; Sato, F.; Kudo, H.; Yoda, S.; Fujihira, M. *Ultramicroscopy* **2004**, *100*, 179–186.

(12) Soppera, O.; Feuillade, M.; Croutxé-Barghorn, C.; Carré, C. *Prog. Solid State Chem.* **2005**, *33*, 233–242.

(13) Jradi, S.; Soppera, O.; Lougnot, D. *J. Microsc.* **2008**, *229*, 151–161.

(14) Zhu, M.; Akari, S.; Möhwald, H. *Nano Lett.* **2001**, *1*, 569–573.

(15) Gigler, A.; Holzwarth, M.; Marti, O. *J. Phys.: Conf. Ser.* **2007**, *61*, 780–784.

\*Corresponding author. E-mail: fernagal@iqm.unicamp.br.

(1) Binnig, G.; Quate, C. F.; Gerber, C. *Phys. Rev. Lett.* **1986**, *56*, 930–933.

(2) Meyer, E.; Heinzlmann, H.; Grütter, P.; Jung, T.; Weisskopf, T.; Hidber, H. R.; Lapka, R.; Rudin, H.; Güntherodt, H. J. *J. Microsc.* **1988**, *152*, 269–280.

(3) Cappella, B.; Dietler, G. *Surf. Sci. Rep.* **1999**, *34*, 1–104.

silanes<sup>7</sup> and blends of nylon-6 and ethylene-*co*-propylene-*co*-diene rubber (EPDM).<sup>8</sup> Meincken et al. used a hydrophilic silicon tip to obtain adhesion maps on the surface of polysulfone membranes<sup>9</sup> and polyurethane coatings<sup>10</sup> with the aim of distinguishing hydrophilic from hydrophobic domains. Other authors<sup>11</sup> applied the pulsed force mode to map adhesive forces on DNA molecules stretched out on a surface using alkane-thiol modified tips and evaluated the influence of the surface topography on the adhesion values measured.

Soppera and colleagues showed the potential of the PFM in analyzing mechanical properties of hybrid sol-gel<sup>12</sup> and acrylic films undergoing photopolymerization.<sup>13</sup> In both cases, the authors established a correlation between the PFM signal and the polymerization degree of the samples. In the first study,<sup>12</sup> the influence of inorganic synthesis parameters and hydrophilic/hydrophobic properties of the sample are evaluated. In the case of acrylic films,<sup>13</sup> they studied the irradiation conditions and the effect of the monomer conversion rate on the film stiffness.

Another interesting application of the technique was to detect single molecules of poly(sodium 4-styrenesulfonate) on rough surfaces using adhesion images.<sup>14</sup> The contrast formed by differences in adhesive forces between the AFM tip and the various domains on the sample surface allowed the identification of small features in rough substrates that are not revealed by topography images. Measurements using the PFM approach were also used to obtain adhesion maps from the entire surface of living HeLa cells.<sup>15</sup>

In the present work, we show results obtained with the PFM mode in the evaluation of surface mechanical properties of thin patterns (less than 100 nm) prepared by drying an aqueous solution of poly(*N*-isopropylacrylamide) and sodium dodecyl sulfate on mica. The features formed by dewetting, when this polymer-surfactant mixture is deposited on the substrate, can be used to template the self-assembly of silica nanoparticles, representing a practical and promising method for nano and micro-fabrication.<sup>16–18</sup>

Images of topography, stiffness, and adhesion together with force-distance curves are presented, yielding information on surface hardness, stiffness, indentation hysteresis, maximum indentation, elasticity modulus, and adhesion force to the AFM tip. Measurements of the adhesion force between the silicon tip and the dewetted mica substrate or the PNIPAM/SDS droplets are especially interesting to this system because they give information on the adhesion forces involved between silica particles and mica or polymer/SDS during the self-assembly/dewetting process. Stronger interaction of the silica particles with the polymer is important to guarantee the success of self-assembly via the dewetting process.

## Materials and Methods

**Sample Preparation.** An aqueous solution containing poly(*N*-isopropylacrylamide) ( $M_w = 90\,000$ ) and sodium dodecyl sulfate (Aldrich) was prepared with the same concentration for polymer and surfactant ( $10^{-4}$  g/mL). PNIPAM was synthesized by free radical polymerization in benzene at 50 °C using azobis(isobutyronitrile) (AIBN) as initiator (used as received from Alfa Chemical). *N*-Isopropylacrylamide monomer (Eastman Kodak Co.) was recrystallized in a mixture of hexane and benzene, and the polymerization was carried out after three cycles of degassing through freezing and thawing. Polymer thin films were prepared

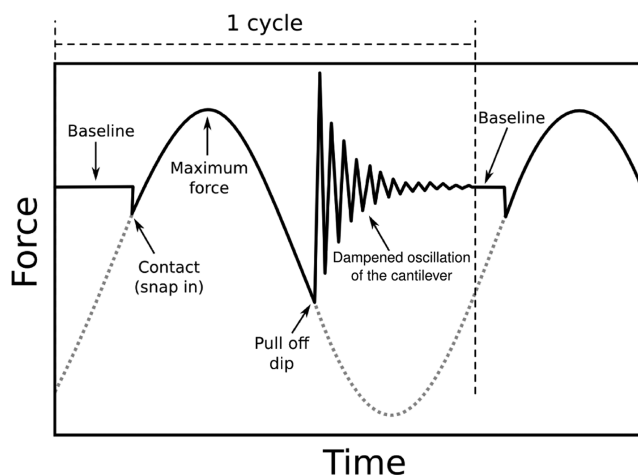


**Figure 1.** Force exerted on the probe when a sinusoidal modulation voltage is applied (dotted line) and the resulting measured force on the probe as it snaps in and out the sample (continuous line). Adapted from ref 19.

by the deposition of 8  $\mu$ L PNIPAM/SDS solution on freshly cleaved mica ( $6 \times 6$  mm<sup>2</sup>) (Ted Pella) and drying within an acrylic chamber under controlled temperature ( $20 \pm 2$ ) °C and relative humidity ( $50 \pm 2$ )%.

**Pulsed Force Mode (PFM).** PFM is an intermittent contact scanning mode in AFM that can be externally coupled to the conventional atomic force microscopes. It modulates the probe frequency and amplitude, so that it oscillates vertically making consecutive tip indentations on the surface.<sup>4,19</sup> Figure 1 shows the force signal exerted on the cantilever as a function of time when a sinusoidal modulation voltage is applied (dotted curve), and the resulting force signal on the cantilever as it snaps in and out of the sample (continuous curve).

Following the signal from left to right, there is initially a baseline, when the tip is far from the sample. When the probe approaches the surface, it is attracted (negative force) and they come into contact, forming the snap-in dip. As the piezo pushes the tip toward the sample (or the sample toward the tip, depending on the equipment), the repulsive force (positive) on the probe reaches a maximum. The maximum force is determined according to the preadjusted set point value and is maintained constant in each indentation cycle during the whole measurement.

As the cantilever is retracted, the force signal decreases until it changes from positive to negative values (repulsive to attractive), and finally, sample and tip lose contact when the force exerted by the equipment to separate probe and sample exceeds the attraction force between them. At this point, we have the second force dip (pull-off or adhesion dip) from which local adhesion is determined. When the tip breaks contact with the sample, the cantilever follows dampened oscillation until the baseline is reached and the cycle restarts.<sup>4,14,19</sup>

In each indentation, a force-distance curve is recorded. At a modulation frequency of 1 kHz, each curve takes 1 ms to be measured, which yields 2000 curves per line at a 0.5 line/s scanning rate. In a typical image (2.2 in and  $300 \times 300$  dpi), ca. 3 force curves per pixel and thus  $4 \times 10^6$  force-distance curves per image are measured. Topography, adhesion, and stiffness maps can be simultaneously obtained using points from the curve specific intervals, called search windows. More information on the PFM working principle and on the search window positions is available in the Supporting Information (Figure S1).

**Sample Analysis.** Topography, stiffness, and adhesion images were obtained on dry samples using an AFM Discoverer TMX 2010 (Topometrix) coupled to an external unit containing

(16) Lee, L. T.; Leite, C. A. P.; Galembek, F. *Langmuir* **2004**, *20*, 4430–4435.

(17) Rezende, C. A.; Lee, L. T.; Galembek, F. *Langmuir* **2007**, *23*, 2824–2828.

(18) Lee, L. T.; da Silva, M. C. V.; Galembek, F. *Langmuir* **2003**, *19*, 6717–6722.

(19) Digital Pulsed Forced mode. User's manual. WITec GmbH, Ulm, Germany, **2005**.

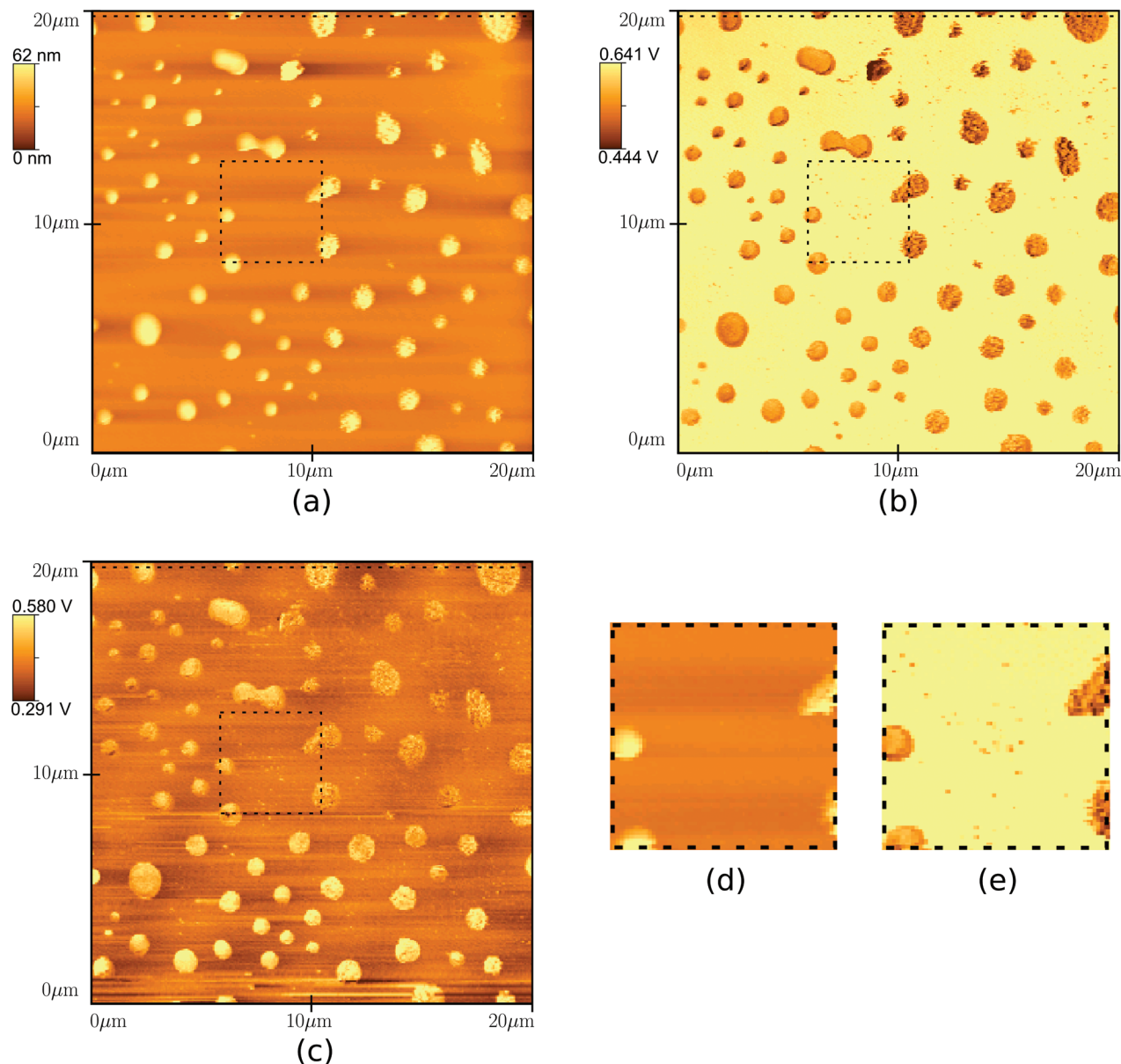


**Figure 2.** PFM images of a PNIPAM-SDS film dewetted from mica at 20 °C: (a) topography, (b) stiffness, and (c) adhesion; and amplified sections (d) and (e) from (a) and (b), respectively. Images from a–c are 20  $\mu\text{m}$  in size. The traced sections show small features on the dewetted substrate that can be more easily observed in the stiffness and adhesion images than in the topography. La, Lb, and Lc are line profiles shown in Figure 3.

the PFM drive from WITec GmbH. The probe used to scan the sample was made of silicon (NCHR-Nanoworld) with  $287 \pm 30$  kHz resonance frequency and  $29 \pm 3$  N/m spring constant. Due to oxidation in contact with air,  $\text{SiO}_2$  groups are formed at the tip surface, and chemical characteristics similar to those of the silica particle surface are expected.<sup>10</sup> The AFM tip used in these measurements has a conical shape at its apex as imaged by scanning electron microscopy (Figure S2 in the Supporting Information).

The  $z$ -piezo of the tube scanner was modulated with a sinusoidal voltage, using a 1 kHz frequency and a 100 mV amplitude. Scanning was carried out at a 10  $\mu\text{m}/\text{s}$  rate (0.5 lines/s) under air and at room temperature. Images were recorded with 20  $\mu\text{m}$   $\times$  20  $\mu\text{m}$  scan size and with  $300 \times 300$  dpi resolution.

## Results and Discussion

**Topography, Stiffness, and Adhesion Images.** Topography, stiffness, and adhesion images, simultaneously obtained on thin PNIPAM-SDS films dewetted from mica surface, are presented in

Figure 2. Line profiles La, Lb, and Lc were traced along line 10 of these images and are presented in Figure 3.

In the topography image (Figure 2a), a pattern formed by droplets containing polymer and surfactant distributed on the substrate can be seen. Droplets of various sizes appear brighter than the substrate. The formation of droplets as the final stage of the dewetting process was reported in studies involving polystyrene films deposited on silicon substrates<sup>20,21</sup> and also in polar films.<sup>18,22</sup> Typical dewetting steps in apolar systems involve film rupture by hole nucleation and growth, both in number and in size, followed by the formation of a polygonal network of liquid rims, that can be more or less regular depending on the system's characteristics.<sup>23</sup> The rims then break due to Rayleigh instability,

(20) Sharma, A.; Reiter, G. *J. Colloid Interface Sci.* **1996**, *178*, 383–399.

(21) Reiter, G. *Phys. Rev. Lett.* **1992**, *68*, 75–78.

(22) Carvalho, A. J. F.; Pereira-da-Silva, M. A.; Faria, R. M. *Eur. Phys. J. E* **2006**, *20*, 309–315.

(23) Oron, A. *Phys. Rev. Lett.* **2000**, *85*, 2108–2111.

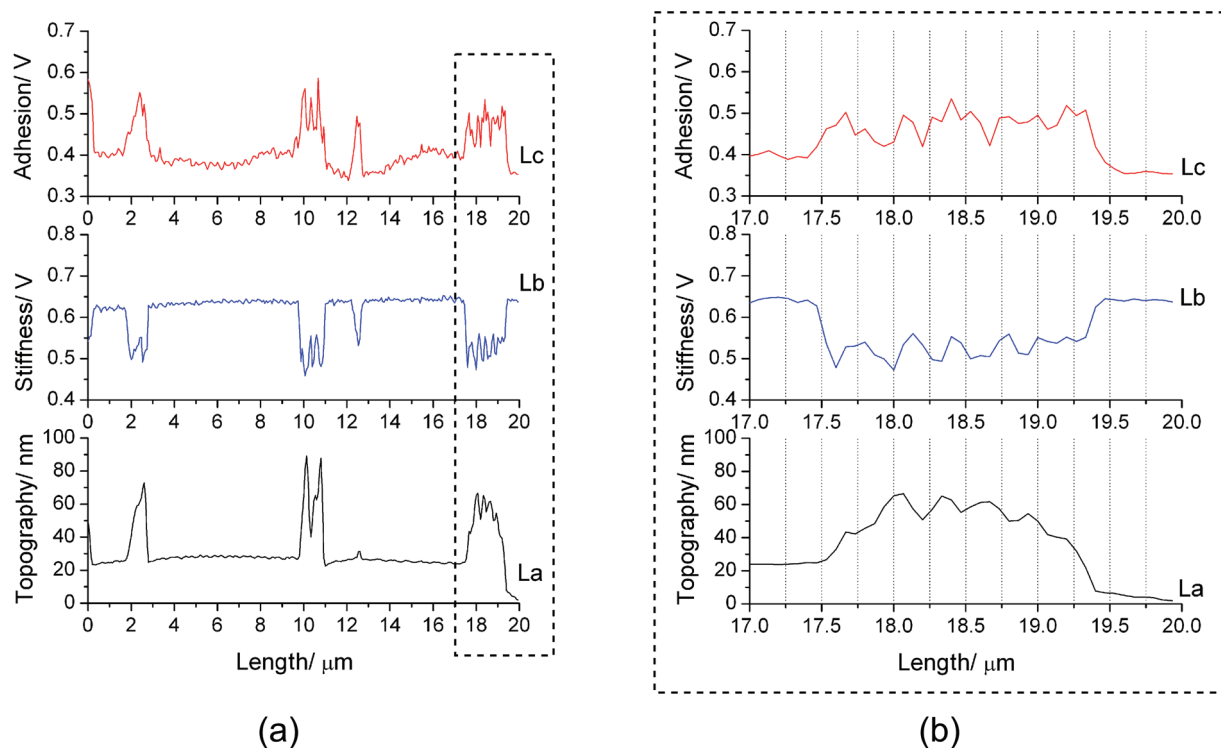


**Figure 3.** Line profiles La, Lb, and Lc traced in line number 10 of images 2a–c: (a) whole line; (b) enlargement of the 17–20  $\mu\text{m}$  region indicated by the traced area in (a).

forming droplets that remain dispersed on the substrate as in Figure 2a.

In the stiffness image (Figure 2b), the dewetted substrate appears brighter (stiffer) than the dry PNIPAM/SDS droplets. According to the slopes obtained from 20 force-indentation curves, the polymer droplets have a  $245 \pm 50$  N/m stiffness, which is much lower than the substrate one ( $2500 \pm 500$  N/m), producing strong image contrast. An interesting aspect of the stiffness image is that it allows the observation of very small droplets in the background, which are hardly observed in the topographic image. This is especially noticeable inside the traced rectangular areas in Figure 2a,b amplified in Figure 2d,e, respectively. The same effect can be observed in the adhesion image, within the traced area in Figure 2c.

The adhesion map (Figure 2c) shows brighter regions corresponding to PNIPAM-SDS droplets that adhere more tightly to the silicon tip than the substrate. The average value of adhesion force on the PNIPAM/SDS droplets is  $428 \pm 32$  nN, while the adhesion measured on the dewetted mica is  $244 \pm 48$  nN. This last value differs from the adhesion force measured in this laboratory for  $\text{Si}_3\text{N}_4$  tips on freshly cleaved mica under ambient conditions (50 nN, in agreement with published data<sup>24,25</sup>), which evidences the presence of an ultrathin PNIPAM/SDS layer left behind on the solid substrate during dewetting.

Adhesion features will be further discussed in the Adhesion section. At this point, it is important to clarify that the sample discussed here consists of two kinds of domains: one is formed by dried droplets containing polymer and surfactant and the other by the dewetted mica substrate, which contains a thin residual layer of the dewetted film. Finally, as the measurements are carried out under ambient conditions (50–60% RH), both sample domains also contain water.

In Figure 2a, some droplets present a rough surface as a consequence of the topographic variations at the film surface formed during the drying/dewetting process. Height variations are clearly observed in the line profile analysis traced on topography images, as shown in line profile La (Figure 3).

According to the image dimension scales, droplets are very flat, about 1  $\mu\text{m}$  in diameter, and maximum height is ca. 60 nm. In such thin structures, late dewetting is expected to occur inside the droplets<sup>17,18</sup> forming heterogeneities at the surface, such as holes that are immobilized when the solvent evaporates, resulting in metastable droplets with a rough aspect.

The rough polymer droplets also present stiffness and adhesion heterogeneities as can be observed in the line profiles Lb and Lc (Figure 3a), where regions with lower voltage correspond to darker areas in the stiffness and adhesion images. Stiffness and adhesion variations in the droplets, however, are more pronounced than topographic variations.

The topographic structure is expected to influence stiffness and adhesion values, since thinner areas of the film (containing less polymer) are stiffer and less adhesive to the AFM tip than the thicker ones. Indeed, thinner areas are more sensitive to the substrate effect; this means that the tip senses the hard substrate after a short penetration in the thin film. However, topography, adhesion, and stiffness traces do not correlate well, as can be observed in the amplified section of the line profiles presented in Figure 3b. This should be related to the droplet nanostructures or to other events involving polymer and surfactant organization within a droplet.

PNIPAM is a thermosensitive polymer with lower critical solution temperature (LCST) around 32  $^{\circ}\text{C}$ . It interacts with SDS above the critical aggregation concentration forming a charged complex that exhibits polyelectrolyte behavior in water.<sup>26</sup> Below the LCST, they form a “necklace” structure in solution,

(24) Thundat, T.; Zheng, X. Y.; Chen, G. Y.; Sharp, S. L.; Warmack, R. J.; Schowalter, L. J. *Appl. Phys. Lett.* **1993**, *63*, 2150–2152.

(25) Eastman, T.; Zhu, D. M. *Langmuir* **1996**, *12*, 2859–2862.

(26) Lee, L. T.; Cabane, B. *Macromolecules* **1997**, *30*, 6559–6566.

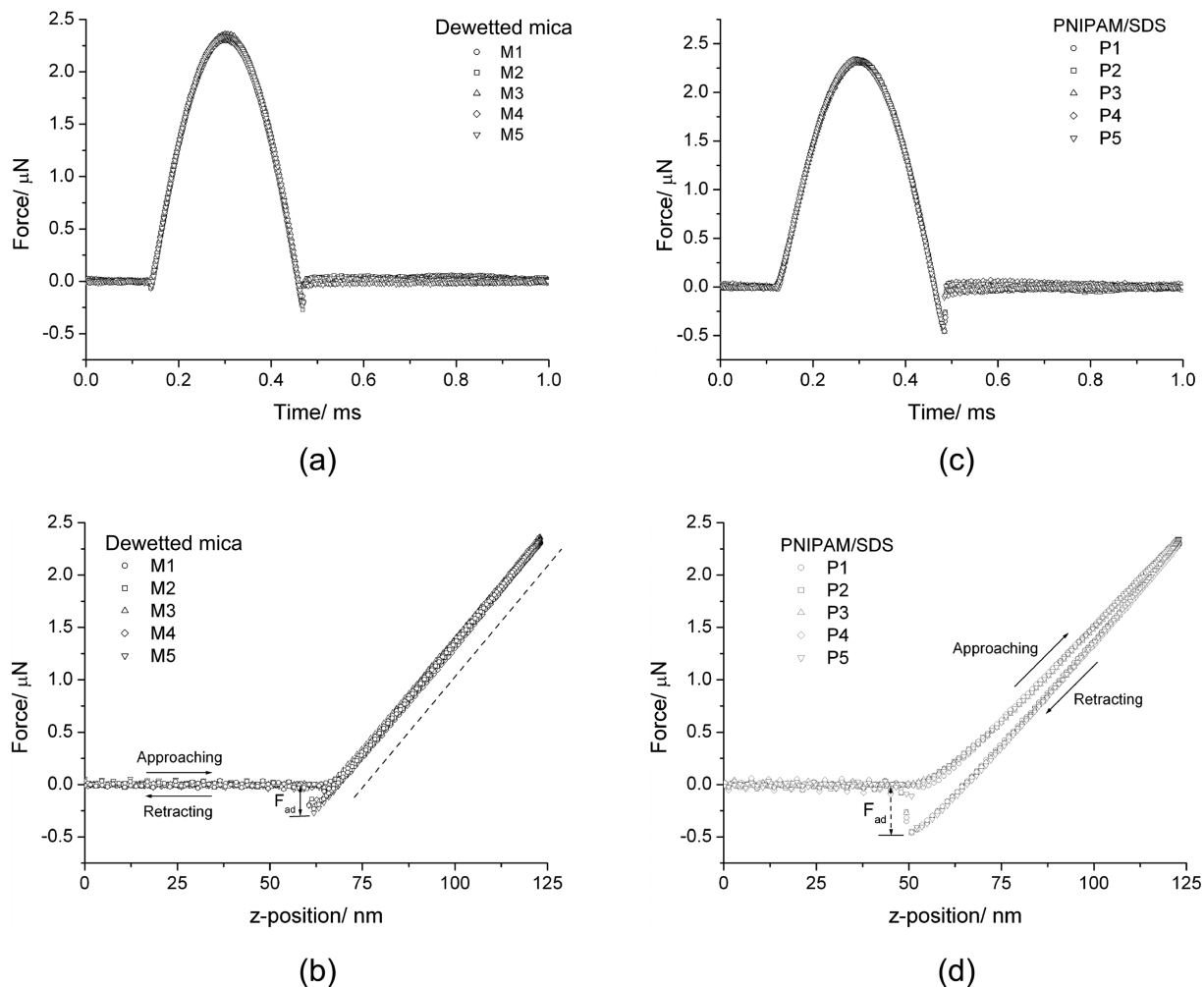


**Figure 4.** Indentation curves on five distinct points on dewetted mica (M1 to M5) and on PNIPAM/SDS droplets (P1 to P5): (a,c) force–time and (b,d) force–cantilever  $z$ -position curves. The traced line in (b) shows the linear variation of the force with the  $z$ -position of the hard substrate and  $F_{ad}$  indicates the adhesion force value in the pull-off dip.

where each macromolecule is decorated with a set of SDS micelles.

While the bulk properties of the PNIPAM/SDS aqueous system are well-known, the same is not observed concerning the structures formed after drying the film. PFM results provide important and new information on the structure of these films and on the dewetting process.

The heterogeneous spots observed inside dried PNIPAM-SDS droplets by stiffness and adhesion PFM images can be understood as the outcome of further phase separation producing domains formed either by surfactant only or having PNIPAM/SDS ratio different from that of the major domains. Therefore, the initial one-phase polymer–surfactant complex is not conserved in the dewetted structure, creating the possibility for further enhanced dewetting.

**Force–Cantilever  $z$ -Position Curves.** Figure 4a,c shows some examples of force–time curves obtained by PFM on dewetted mica and on the PNIPAM-SDS droplet domains, respectively. The original raw data provided by the PFM software (in time units) can be converted to distance (or position of the cantilever in the  $z$ -direction), considering the sinusoidal path of the cantilever, where its position  $z(t)$  depends on the  $A_{PFM}$

amplitude and on the  $\nu$  frequency applied by the PFM device, at time  $t$  and phase angle  $\phi$ .<sup>27</sup>

$$z(t) = A_{PFM} \cos(2\pi\nu t + \phi) \quad (1)$$

The cantilever position in  $z(t)$ , which is the quantity obtained during a force–distance experiment, is not the real tip–sample distance ( $D$ ), due to the contributions from the cantilever deflection ( $\delta_c$ ) and the sample deformation ( $\delta_s$ ) ( $z = D + \delta_c + \delta_s$ ).<sup>3</sup>

Using these relationships, the force–distance curves presented in Figure 4b,d are calculated from Figure 4a,c, for indentations on dewetted mica and on the PNIPAM-SDS droplets. Five randomly chosen curves from different points in each of these two kinds of domains are superimposed, and they show good reproducibility. The traced line parallel to the dewetted mica curves in Figure 4b highlights the linear variation of the force with the cantilever position, indicating elastic behavior during tip approximation and retraction on the hard substrate in the observed range of  $z$ -positions.

In Figure 5a, two typical force–distance curves (continuous curve on dewetted mica and scattered curve on PNIPAM/SDS droplets) are plotted together for easier comparison. Following the curves from left to right, a constant zero force is measured as the tip approaches the surfaces until they come into contact. On average, the contact point occurs when the cantilever position is ca. 50 nm on the PNIPAM-SDS curve and 66 nm on dewetted

(27) Gigler, A. M. *Dynamic Investigation of Polymeric Materials – Reproducible Data Acquisition and Profound Mechanical Analysis*; Doctorate Thesis; Ulm University, Ulm, Germany, 2006.

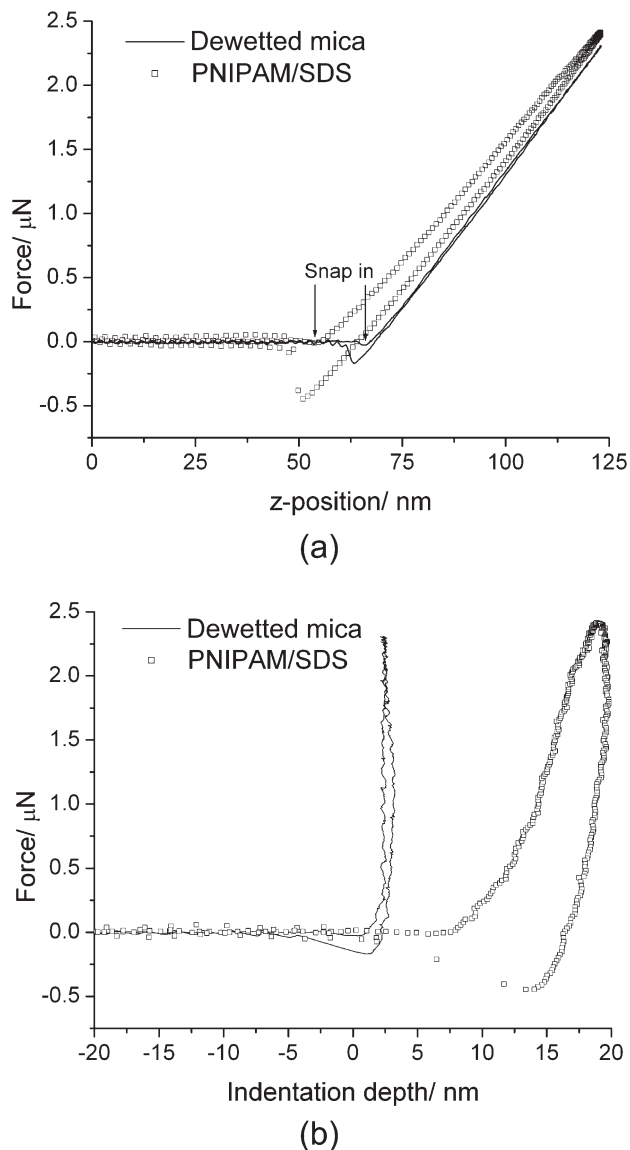


**Figure 5.** (a) Force–cantilever  $z$ -position and (b) force–indentation depth curves obtained by PFM on dewetted mica and on PNIPAM/SDS droplets.

mica curve. The 16 nm difference is nearly one-half the droplet maximum average height, which is about 30 nm, and it is consistent with the fact that tip indentation can occur at any point on the droplet surface.

The contact region appears as a small snap-in dip that is quite clear in this curve for dewetted mica, but that is not as well-defined in the whole set of analyzed curves on the sample. The snap-in dip can be observed when the attractive force gradient is larger than the spring constant of the tip.<sup>3</sup> When the approaching tip gets close to the surface, it is suddenly pulled into contact, causing a dip in the force–distance curve. In this work, however, cantilevers with a relatively high spring constant (29 N/m) were used to enhance the quality of the stiffness images, and the snap-in dip cannot always be detected.

The interaction force increases up to a maximum of approximately 2.3  $\mu\text{N}$  for both PNIPAM/SDS droplets and the dewetted mica. In the case of mica, the hysteresis in the approach–retraction cycle is almost nil, but it is very significant in the PNIPAM/SDS curves, as seen in Figure 5a. Higher hysteresis on the PNIPAM/SDS droplets is a consequence of the viscoelastic

behavior of the polymer. Due to tip penetration, the polymer chains can deform and flow, dissipating energy, and undergoing deformation. Force in both indentation and retraction paths of the curve will then differ. Average values of snap-in position and maximum indentation force on dewetted mica and on PNIPAM/SDS droplets are presented in Table 1.

**Force–indentation Depth Curves.** From the cantilever  $z$ -position values ( $z$ ), it is possible to calculate the indentation of the cantilever on the sample ( $\delta_s$ ), considering the snap-in position and the cantilever deformation contribution ( $\delta_c$ ). The latter can be extracted from the slope of the linear part of the force– $z$  position curve in an indentation on a hard substrate (Figure 4b). As the mica surface is too hard to deform ( $\delta_s = 0$ ), the total deformation is assumed to be equal to the cantilever deformation.

Force–indentation depth curves on PNIPAM-SDS droplets and on the dewetted mica substrate are presented in Figure 5b. The mica curve has two characteristics that are typical of an elastic stiff material: the large slope at the loading side of the curve and the very low hysteresis. The high slope of the indentation curve results in very small values of maximum indentation on dewetted mica. The values presented in Table 1 for indentation at maximum force ( $\delta_{F_{\max}}$ ) ( $2.7 \pm 0.7$  nm) and maximum indentation ( $\delta_{\max}$ ) ( $3.3 \pm 0.7$  nm) on dewetted mica are mainly a consequence of tip indentation on the thin residual layer adsorbed on the surface than on mica itself.

On the other hand, a smaller slope and much higher loading–unloading hysteresis, together with deeper maximum indentation (almost 20 nm) can be observed on the curves recorded on the polymer.

Quantitative values can be extracted from these curves for the energy dissipated by hysteresis, the postflow distance, remanent depth, adhesion force, detachment distance, and energy as shown in Figure 6 in one of the experimental curves. Detailed definitions for these parameters can be found in the Supporting Information section. Other characteristic values such as sample hardness, compliance, and Young’s modulus are also calculated. All the calculated values are presented in Table 1. Averages and standard deviations were obtained from 20 randomly chosen curves on the PNIPAM/SDS droplets and 20 curves on the dewetted mica substrate.

**Plastic Deformation.** Table 1 shows values of remanent depth left on the substrate that are much larger on the PNIPAM-SDS droplets ( $13.3 \pm 2.3$  nm) than on the dewetted mica substrate ( $1.2 \pm 0.4$  nm), which is coherent with the small indentation of the tip on this harder material.

The difference between  $\delta_{F_{\max}}$  and  $\delta_{\max}$  in these samples is very small, within the standard deviation ranges, which results in postflow distance values close to zero. This behavior is expected on mica, but not on the PNIPAM/SDS droplets. In purely elastic materials,  $\delta_{F_{\max}}$  and  $\delta_{\max}$  should coincide, while in viscoelastic materials, the tip can still keep indenting on the sample after the maximum force peak and a postflow distance is often observed. In the case of PFM experiments, indentation time is very short, and it is possible that the polymer postflow may not be detected at the high indentation frequency used.

On the other hand, the mixed elastic–plastic behavior of the polymer is very clear when we consider the energy dissipated by hysteresis in each approximation–retraction cycle. The average hysteresis value measured by indenting on dewetted mica is very small ( $1.0 \pm 0.2 \cdot 10^{-15}$  J), considered as inherent to all measurements. It is attributed to variations in the determination of the cantilever position and to a thin adsorbed layer containing residual polymer from dewetting or other contaminants from air. The hysteresis measured on PNIPAM/SDS droplets is about

**Table 1. Surface Mechanical Parameters Obtained by PFM on the PNIPAM/ SDS Droplets and on the Dewetted Mica Substrate (Used As a Reference)<sup>a</sup>**

parameter	PNIPAM/SDS	dewetted mica
snap-in position/ nm	50.4 ± 2.9	66.2 ± 1.1
maximum force/ μN	2.31 ± 0.05	2.33 ± 0.03
stiffness/ N/m	245 ± 50	2500 ± 500
remnant depth/ nm	13.3 ± 2.3	1.2 ± 0.4
indentation at maximum force ( $\delta_{F_{\max}}$ )/ nm	18.7 ± 2.9	2.7 ± 0.7
maximum indentation ( $\delta_{\max}$ )/ nm	19.2 ± 3.1	3.3 ± 0.7
hysteresis/ $10^{-15}$ J	11.5 ± 1.7	1.0 ± 0.2
hardness/ GPa	3.3 ± 0.1	7.4 ± 0.1
compliance/ N/m	182 ± 22	2150 ± 700
adhesion force/ nN	428 ± 32	244 ± 48
detachment distance/ nm	4.8 ± 2.0	9.8 ± 1.4
Detachment energy/ $10^{-15}$ J	4.0 ± 0.3	1.3 ± 0.3
Young modulus/ GPa	0.7 ± 0.2	12.5 ± 7.8

<sup>a</sup> Mean values and standard deviation are averages of 20 indentation curves measured on each kind of domain.

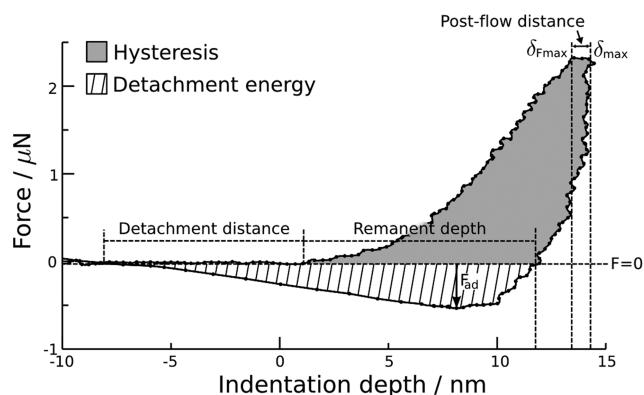


**Figure 6.** Scheme showing how the values of postflow distance, hysteresis, adhesion force ( $F_{ad}$ ), remanent depth, and detachment energy and distance are obtained from a force-indentation depth curve.

eleven times higher ( $11.5 \pm 1.7 \times 10^{-15}$  J), and the values are comparable to hysteresis in indentation curves measured by Gigler,<sup>27</sup> using the same technique. This author calculated  $(0.30 \pm 0.02) \times 10^{-15}$  J energy dissipated by hysteresis on poly(methyl methacrylate) (PMMA) surface,  $(5.2 \pm 0.04) \times 10^{-15}$  J on styrene butadiene rubber (SBR), and hysteresis very close to zero on silicon.

**Hardness and Compliance.** The hardness ( $H$ ) of the surface can be estimated by dividing the maximum indentation force ( $F_{\max}$ ) by the contact area ( $A$ ) projected at the surface:<sup>28,29</sup>

$$H = \frac{F_{\max}}{A} \quad (2)$$

and  $A$  can be calculated by  $\pi R^2$  (the cross section area of the cone) with  $R = 15$  nm for a 20 nm indentation and  $R = 10$  nm for indentations smaller than 10 nm.

Sample compliance can also be calculated, since it is defined as the ratio between the maximum indentation force and the maximum indentation value

$$D = \frac{F_{\max}}{\delta_{\max}}$$

Average hardness is  $3.3 \pm 0.1$  GPa in the polymer-surfactant droplets and  $7.4 \pm 0.1$  GPa on dewetted mica. No experimental

results were found in literature to compare these nanohardness values for the dewetted substrate or the polymer droplets. Some authors,<sup>29</sup> using computational simulations, calculated values from 30 to 50 GPa for nanoindentations of AFM sharp and flat tips on the different surfaces of silicon wafers. These simulated values, however, were obtained using very small projected contact areas (indentation depths from 0.4 to 1.8 Å). This explains the greater hardness in comparison to our results, which were calculated using an experimental value ca. 30 Å for maximum indentation on mica. For macroindentations using Vickers indenter, hardness for silicon wafers were measured in the 9–12 GPa range.<sup>30</sup>

The contact area projected on the surface is a very important parameter to be defined when we measure hardness. In nanoindentations using a conical tip with small cone angle (almost a cylinder), as in this experiment, the contact area projected on the surface (tip cross section) does not change significantly even when the indentation depth does. The hardness can be thus overestimated for great indentation depths, when the real contact area is much larger than the tip cross section. This can be the case in this work for hardness values calculated on polymer-surfactant droplets.

So, perhaps in this system, the compliance ( $D$ ) is more suitable to characterize sample hardness, since it considers the significant differences in indentation depth in each domain. Sample compliance was calculated as  $182 \pm 33$  N/m on PNIPAM-SDS droplets and  $2150 \pm 700$  N/m on the dewetted substrate.

**Adhesion.** The adhesion force is higher on the polymer droplets ( $428 \pm 32$  nN) than on dewetted mica ( $244 \pm 48$  nN). The measured values of adhesive force have contributions from a sum of van der Waals forces and H-bond interactions, but they are dominated by capillary forces. Yet, adhesion values include important contribution from the tip-sample contact area, which is greater in the viscoelastic deformed polymer droplets than in the case of flat contacting surfaces.

Capillary forces are well-known as the most important forces involved in tip-sample interactions in air.<sup>31</sup> They exceed all other forces, and in particular, they mask van der Waals forces, so that, in order to measure surface forces without the influence of capillary adhesion,<sup>32</sup> immersion in a liquid environment or very low humidity conditions are required.

Typical adhesion forces between a  $\text{Si}_3\text{N}_4$  tip and mica are 40–70 nN when measured in air under 20–90% relative humidity<sup>24,25</sup>

(30) Puech, P.; Demangeot, F.; Pizani, P. S. *J. Mater. Res.* **2004**, *19*, 1273–1280.

(31) Weisenhorn, A. L.; Hansma, P. K.; Albrecht, T. R.; Quate, C. F. *Appl. Phys. Lett.* **1989**, *54*, 2651–2353.

(32) Valadares, L. F.; Linares, E. M.; Bragança, F. C.; Galembeck, F. J. *Phys. Chem. C* **2008**, *112*, 8534–8544.

(28) Oliver, W. C.; Pharr, G. M. *J. Mater. Res.* **2004**, *19*, 3–20.

(29) Astala, R.; Kaukonen, M.; Nieminen, R. M.; Heine, T. *Phys. Rev. B* **2000**, *61*, 2973–2980.

and 1.4 nN within a water cell.<sup>3</sup> This last value is assigned to van der Waals forces only. In the present work, a 50 nN adhesion force was measured for a similar tip on bare mica under 55% RH, in agreement with published values. The difference in adhesion forces in dewetted ( $244 \pm 48$  nN) and freshly cleaved mica (50 nN) reveals the presence of an ultrathin PNIPAM layer left behind on dewetted mica, as expected considering previous reports in the literature.<sup>33–35</sup>

The strength of chemical bonds is usually expressed as the energy ( $E_b$ ) involved in this bonding. Bonding energy and force ( $F_b$ ) are related by the bond distance ( $l$ ) as  $E_b = lF_b$ . Typical energy values involved in van der Waals interactions (dispersion and dipole–dipole) are in the 0.1–10 kJ/mol range, and for hydrogen bonding, they are between 10 and 40 kJ/mol.<sup>36</sup> As the typical bond length for these interactions is about 2–10 nm,<sup>3</sup> individual van der Waals force values between 0.02 and 10 pN and hydrogen bonding interaction in the range 10–30 pN can be found.

Williams et al.<sup>37</sup> measured adhesion forces with mean intensity ranging from 3.6 to 15.6 nN for indentations with a  $\text{Si}_3\text{N}_4$  tip on mica in water environment and attributed this total force to hydrogen bonds between the tip and the substrate. They also used a method based on Poisson's distribution to estimate the force of each hydrogen bond, and thus, a 181 pN value was obtained.

The difference in adhesion force between the silicon tip and the polymer droplets ( $428 \pm 32$  nN) or the dewetted mica ( $244 \pm 48$  nN) reveal different interaction affinities between these two domains and the silica. This information is also important in other systems containing these three components. In previous studies of this research group,<sup>17,38</sup> different interactions of silica nanoparticles with mica and with polymer/SDS film influenced the self-assembly behavior of these particles. When a dispersion of silica particles in PNIPAM/SDS solution dewets the mica substrate, the polymer forms patterns within which particles get confined and organized. Low adhesion to the substrate and high adhesion to the polymer film are essential to allow good confinement of the particles inside the film, a required condition for the success of the self-organization process. Silicon tip and silica particle surfaces can be assumed to have similar interactions with dewetted mica and polymer, since silicon tips are usually oxidized in contact with air.<sup>10,39</sup>

Adhesion properties of the sample are also related to the detachment distance and to the energy involved in the detachment. The detachment distance is  $4.8 \pm 2.0$  nm on PNIPAM/SDS droplets and  $9.8 \pm 1.4$  nm on dewetted mica. This distance can indicate the ability of the surface to deform as the tip moves away from it, including the effect of adsorption layers. PNIPAM/SDS droplets are expected to be more deformable than mica and to present lower effect of adsorbed water than clean mica, which is highly hydrophilic. PNIPAM, on the other hand, exhibits only a partial hydrophilic/hydrophobic character, since it is water-soluble below the LCST, but it can also adsorb to the air–water interface.<sup>26,38,40</sup> Besides, the presence of the residual film on dewetted mica should also be accounted in this case. All these contributions are involved in the detachment distance value.

In terms of energy, detachment energy is approximately 3 times larger on PNIPAM-SDS droplets ( $4.0 \pm 0.3 \times 10^{-15}$  J) than on

dewetted mica ( $1.3 \pm 0.3 \times 10^{-15}$  J). Detachment distance and energy values analyzed together show that, although the detachment distance is larger on the dewetted mica substrate than on the polymer droplets, the stronger tip–sample adhesion interactions and the polymer ability for plastic deformation in the second case result in higher detachment energy.

**Young's Modulus.** Young's modulus values ( $E$ ) were calculated using the model proposed by Johnson–Kendall–Roberts (JKR) that is based on the effect of adhesion force on the contact radius between the indenter and the surface.<sup>41</sup> This model is suitable to describe the behavior of highly adhesive systems with low stiffness and variable tip radius.<sup>3,27,42,43</sup> The radius of contact ( $a$ ) between the tip and the sample is given by

$$a^3 = \frac{R}{E_r} \left( F + 3W\pi R + \sqrt{6W\pi R F + (3W\pi R)^2} \right) \quad (3)$$

where  $R$  is the tip radius,  $F$  is the tip–sample interaction force,  $W$  is the adhesion work, and  $E_r$  is the reduced modulus that is related to the Young's modulus ( $E$ ) and the Poisson ratio ( $\nu$ ) of the surface (s) and the indenter (i)

$$\frac{1}{E_r} = \frac{(1 - \nu_s^2)}{E_s} + \frac{(1 - \nu_i^2)}{E_i} \quad (4)$$

At the pull-off dip, the adhesion force  $F_{ad}$ , the contact radius  $a_{ad}$ , and the sample deformation  $\delta_{ad}$  are defined as

$$F_{ad} = \frac{3}{2} W\pi R \quad (5)$$

$$a_{ad} = \left( \frac{3}{2} \frac{W\pi R^2}{E_r} \right)^{1/3} \quad (6)$$

$$\delta_{ad} = \left( \frac{W^2 \pi^2 R}{12 E_r^2} \right)^{1/3} \quad (7)$$

According to the JKR model, the work of adhesion between the tip and the sample was calculated as  $9.1 \pm 0.7$  N/m on PNIPAM/SDS and  $5.2 \pm 1.0$  N/m on dewetted mica. Using the values of sample deformation in the pull-off dip and  $R = 10$  nm,  $E_r$  and then  $E_s$  for mica and for PNIPAM/SDS were calculated using  $\nu_i = 0.15$  (silicon tip),  $\nu_{mica} = 0.17$ ,  $\nu_{pol} = 0.4$ , and  $E_i = 160$  GPa.<sup>27,44,45</sup>

On dry PNIPAM-SDS droplets,  $E$  is calculated as  $0.7 \pm 0.2$  GPa. In the literature, there is no comparable data other than figures for highly swollen cross-linked aqueous PNIPAM hydrogels (12 Pa to 1.5 MPa).<sup>46–49</sup> For a solid polymer such as

(41) Johnson, K. L.; Kendall, K.; Roberts, A. D. *Proc. R. Soc. Lond.* **1971**, *324*, 301–313.

(42) Wu, K. C.; You, H. I. *Appl. Surf. Sci.* **2007**, *253*, 8530–8537.

(43) Ha, J. L.; Fung, R. F.; Chen, Y. C. *J. Dynam. Syst. Meas. Control* **2005**, *127*, 705–709.

(44) Mantell, C. L. *Engineering Materials Handbook*; McGraw-Hill: New York, 1958.

(45) Brandrup, J.; Immergut, E. H. *Polymer Handbook*; Wiley Interscience: New York, 1975.

(46) Ohya, S.; Kidoaki, S.; Matsuda, T. *Biomaterials* **2005**, *26*, 3105–3111.

(47) Cheng, X. H.; Canavan, H. E.; Stein, M. J.; Hull, J. R.; Kveskin, S. J.; Wagner, M. S.; Somorjai, G. A.; Castner, D. G.; Ratner, B. D. *Langmuir* **2005**, *21*, 7833–7841.

(48) Wiedemair, J.; Serpe, M. J.; Kim, J.; Masson, J. F.; Lyon, L. A.; Mizaikoff, B.; Kranz, C. *Langmuir* **2007**, *23*, 130–137.

(49) He, Q.; Kueller, A.; Schilp, S.; Leinsten, F.; Kolb, H. A.; Grunze, M.; Li, J. B. *Small* **2007**, *3*, 1860–1865.

(33) Sharma, A. *Langmuir* **1993**, *9*, 861–869.

(34) Sharma, A.; Khanna, R. *Phys. Rev. Lett.* **1998**, *81*, 3463–3466.

(35) Seemann, R.; Herminghaus, S.; Jacobs, K. *Phys. Rev. Lett.* **2001**, *86*, 5534–5537.

(36) Israelachvili, J. N. *Intermolecular and Surface Forces*, 3rd ed.; Academic Press: New York, 1989.

(37) Williams, J. M.; Han, T.; Beebe, T. P., Jr. *Langmuir* **1996**, *12*, 1291–1295.

(38) Rezende, C. A.; Lee, L. T.; Galebeck, F. *Langmuir* **2008**, *24*, 7346–7353.

(39) Bruch, L. W. *Phys. Rev. B* **2005**, *72*, 033410/1–3.

(40) Jean, B.; Lee, L. T.; Cabane, B. *Langmuir* **1999**, *15*, 7585–7590.



polystyrene, an  $E$  value equal to  $3.37 \pm 0.52$  GPa was calculated using JKR analysis for data obtained by AFM tip indentation on a solid substrate.<sup>50</sup>

In the case of the dewetted mica substrate, the average value calculated for  $E$  is  $12.5 \pm 7.8$  GPa, which is in agreement with values from the literature for bare mica Young modulus.  $E$  values obtained in experimental macroscopic indentations lie between 15 and 20 GPa,<sup>44</sup> and in the case of nanoindentation of a silicon AFM tip on mica, Kaul and colls<sup>51</sup> calculated an  $E$  value equal to 5.6 GPa using Sneddon's analysis (that does not consider adhesive interactions).<sup>52</sup> Even though the average is within the expected ranges, the spread of these measurements is very large, showing that the thin layer on dewetted mica surface is inhomogeneous.

### Conclusion

PNIPAM-SDS films dewetted from mica substrate show flat droplets within a broad radius range. PFM revealed heterogeneous features inside the PNIPAM/SDS droplets that were observed on the adhesion and stiffness images. The heterogeneous spots are assigned to phase separation of the polymer–surfactant complex during the drying/dewetting process. These images also revealed some very small droplets formed on dewetted areas, which could scarcely be observed by noncontact imaging and that show how the sensitivity of this technique helps detecting minute surface features. Finally, the presence of a very thin layer containing polymer and surfactant left on mica after dewetting was revealed by comparing adhesion force values measured on dewetted and freshly cleaved mica.

(50) Lubarsky, G. V.; Davidson, M. R.; Bradley, R. H. *Surf. Sci.* **2004**, *558*, 135–144.

(51) Kaul, A. D.; Gangwal, A.; Wadhwa, S. S. *Curr. Sci.* **1999**, *76*, 1561–1566.

(52) Sneddon, I. N. *Int. J. Eng. Sci.* **1965**, *3*, 47.

The contrast in stiffness images is especially good due to the significant stiffness difference calculated for both components ( $245 \pm 50$  N/m on the polymer and  $2500 \pm 500$  N/m on dewetted mica). Adhesion force and detachment energies of the AFM tip are respectively  $(428 \pm 32)$  nN and  $(4.0 \pm 0.3) \times 10^{-15}$  J on the polymer droplets and  $(244 \pm 48)$  nN and  $(1.3 \pm 0.3) \times 10^{-15}$  J on the dewetted substrate. These values can be assigned to capillary forces due to water, surfactant, and the polymer film at the sample surface and also to van der Waals forces and hydrogen bonding.

Young's modulus ( $E$ ) is  $(0.7 \pm 0.2)$  GPa on polymer/SDS droplets, which is close to the value obtained in nanoindentations on polystyrene,  $(3.37 \pm 0.52)$  GPa.<sup>50</sup> In the case of the dewetted mica substrate, the values calculated for  $E$  are in agreement with values in the literature for bare mica.<sup>44,51</sup> The spread of these results is related to heterogeneous areas on dewetted mica surface covered with various amounts of adsorbed solutes resulting from dewetting.

This work shows that PFM produces a wealth of nanomechanical data, both concerning the number of measured parameters and the number of individual measurements, which makes this technique very suitable for complex surfaces such as those formed by dewetted films.

**Acknowledgment.** The authors thank Dr. Alexander Gigler (LM - University of Munich) for the great help in the data treatment for obtaining the force–distance curves and the Brazilian foundations FAPESP, CNPQ and CAPES for the financial support.

**Supporting Information Available:** Search windows on the PFM curves; scanning electron microscopy image of the AFM tip; definitions of the mechanical parameters obtained from force–indentation depth curves; sequential topography images of a sample area. This material is available free of charge via the Internet at <http://pubs.acs.org>.